Date of publication xxxx 00, 0000, date of current version xxxx 00, 0000.

Digital Object Identifier

A New Family of Reconfigurable Waveguide Filters and Diplexers for High-Power Applications

JUAN C. MELGAREJO[1], JAVIER OSSORIO[1], SANTIAGO COGOLLOS[1], (Member, IEEE), MARCO GUGLIELMI[1], (Life Fellow, IEEE), ÁNGEL A. SAN-BLAS[2], JOAQUÍN F. VALENCIA[1], ANA VIDAL[1], (Member, IEEE), TILLMAN TRONSER[3], AND VICENTE E. BORIA[1], (Fellow, IEEE)

[1]iTEAM Group, Departamento de Comunicaciones, Universitat Politècnica de València, 46022 Valencia, Spain (e-mail: juamelle@teleco.upv.es, jaosgar@teleco.upv.es, sancobo@dcom.upv.es, marco.guglielmi@iteam.upv.es, joavasu2@teleco.upv.es, avidal@dcom.upv.es, vboria@dcom.upv.es)
[2]Department of Communications Engineering-I3E, Miguel Hernández University of Elche, 03202 Elche, Spain (e-mail: aasanblas@umh.es)
[3]Tronser GmbH, 75179 Pforzheim, Germany (e-mail: tillmann@tronser.com)

Corresponding author: A. A. San-Blas (e-mail: aasanblas@umh.es).

This work was supported by the Ministerio de Ciencia e Innovación, Spanish Government, through the Subprojects C43 and C41 of the Coordinated Research and Development Project PID2019-103982RB under Grant MCIN/AEI/10.13039/501100011033.

ABSTRACT In this paper, we discuss how the use of the recently developed modified tuning pin (MTP) can be extended to the design of filters and diplexers implemented in rectangular waveguide, that can be reconfigured in a number of discrete states, and that can be used in high-power payloads. As an application example, the design of two reconfigurable filters and a reconfigurable diplexer is fully described. The high-power behavior of these components (in particular, with respect to corona and multipaction effects) is also studied in detail, in order to demonstrate that the structures that we discuss can operate correctly under high-power conditions. Furthermore, comparisons between simulations and measurements of several prototypes are also included, showing an excellent agreement between simulated and experimental data, thereby fully validating both the design approach and the filter reconfiguration strategy.

INDEX TERMS Microwave filters, microwave diplexers, passive components, reconfigurable, rectangular waveguide, remote operation, high-power.

I. INTRODUCTION

MODERN communication payloads are currently moving toward systems with channels that can be reconfigured to accommodate changing customer demands. As a consequence, significant research effort is currently devoted to the development of new tunable or reconfigurable filter structures. In this context, an excellent review of the most recent techniques for designing tunable filtering devices, and the related achievements, has recently been published in [1].

Standard bandpass filters and diplexers, are very commonly used in the output network of many communication satellites and in many other applications that require high-power microwave signals. As a consequence, the high-power behavior of the reconfigurable components under development needs to be studied in detail (in particular, with respect to corona and multipaction effects), in order to ensure that the structures can operate correctly under high-power conditions (that is, with more than 200 Watts signals).

Furthermore, filtering devices that can be tuned or reconfigured, can be, generally, divided into two large groups: structures based on the use of *active* elements (such as varactors, PIN diodes, or other semiconductor devices), and *passive* structures based on the use of moving parts (such as metallic or dielectric tuners, MEMS devices, or other moving elements). Filtering devices that include active elements in the main path of the microwave signal are clearly not suitable for high-power applications. The ones based on moving parts, on the other hand, may indeed be suitable for high-power operation. However, the use of moving parts can result in small gaps when tuning resonators toward the lower frequency end of the tuning range, or when reconfiguring the filter toward wider bandwidths. Smaller gaps are normally associated with high electromagnetic fields which, in turn, may strongly reduce the maximum allowed signal power before corona or

multipaction effects can be initiated. The suitability for high-power applications must, therefore, be studied in detail for each specific design.

Before describing the reconfigurable structures that are the subject of this paper, however, we find it important to discuss the results of our review of past relevant publications in the context of tunable and reconfigurable filters. However, for the reason stated above, our review will focus only on *passive* tunable and reconfigurable structures.

One possibility to obtain continuous reconfigurable filters is to physically change the size of its cavities. In [2] and [3], for example, two adjustable end walls were used to modify the volume of the cavities of a filter. Using the same method, a reconfigurable output multiplexer was designed in [4].

Another common alternative to design reconfigurable filters is to use dielectric or metallic screws (or tuners) to change the resonators electric field. In this context, a study on the maximum tuning range of filters often employed in satellite payloads (using circular and rectangular waveguide technology) was carried out in [5]. Another example is [6], where the tuning range of an inductive waveguide filter using teflon rods was studied. Both [5] and [6] use tuning elements inside the coupling apertures to obtain tunable coupling levels as well. More recently, dielectric resonator filters with multiple reconfigurable passbands are designed in [7] using tuning screws placed in different positions, and an artificial neural network optimization method is used in [8] for designing tunable bandpass filters. Another recent work uses a mode-switching concept to design band-reconfigurable bandpass filters by means of a pair of tuning screws [9], while the work presented in [10] focuses on the design of tunable filters and diplexers based on in-line dual-post structures. Although these last two papers do propose very interesting solutions, they do not discuss the behavior of the filters under high-power excitation.

Yet another approach is to use tunable, non-resonating cavities to replace the classic coupling windows [11], [12]. The cavities operate as impedance inverters since their resonance frequencies are outside of the filter bandwidth.

Integrating mechanical switches and microwave filters is another traditional method of implementing flexible input/output networks for communication payloads [13]. The switches are primarily based on rotating mechanisms [14], semiconductor technology, or MEMS [15], [16], [17], [18], [19].

Finally, two additional interesting approaches can also be found in the area of tunable and reconfigurable filters, namely, [20] and [21]. In [20], a structure with a reduced number of tuning elements is proposed to implement microwave filters that can be tuned both in terms of center frequency and bandwidth. However, the solution discussed is applicable only to filters implementing a Butterworth transfer function. In [21], a clever system is discussed where a single tuning mechanism can be used to control the center frequency of a coaxial filter and a diplexer. However, the filters can only be tuned in terms of center frequency and have a fixed bandwidth.

At this point, however, it is important to note that, in our review of the state-of-the-art, we have not identified any contribution that specifically discusses the use of tunable and (or) reconfigurable filter structures specifically developed for high-power microwave signals.

Recently [22], a novel device that combines the capabilities of a microwave filter and waveguide switch (F&S) has been proposed. The key aspect of the F&S is a modified tuning pin (MTP). The MTP can be used to activate and deactivate the resonant cavities, and coupling apertures, to generate different paths for the signal. One key feature of the MTP is that the position of the pin does not need to be set with extreme accuracy to deactivate cavities or couplings. As a result, the pin can be very effectively moved with computer controlled low-accuracy actuators, thereby allowing for remote operation at a very reasonable cost.

In this context, therefore, the main innovative contributions of our paper is to provide a proof-of-concept for how the use of the MTPs, first introduced in [22], can effectively be extended to additional reconfigurable devices of practical interest, such as filters and diplexers, that can operate in a number of discrete states, and that are suitable for high-power operations.

To continue, it is now important to note that, currently, the reconfiguration of the front end of telecommunication satellites (for instance) is achieved using rotary switches in waveguide technology to connect waveguide filters to each other in order to implement the desired functionality. However, the use of a single commercial rotary switch in WR-75 waveguide, for instance, may result in about 500 g of additional weight, would require about 325.000 mm^3 of additional volume, and would cost several thousand dollars. The solution that we propose, on the other hand, is based on the use of microwave filters that include MTPs in their structures. The MTPs are mechanically very simple, light, and can be operated with low-cost actuators. Furthermore, the MTPs are completely removed from the cavities when the filters are operational, and the filters themselves do not contain any moving parts. As a result, using the devices that we discuss in the output network of high-power microwave payloads, may result in very significant savings in terms of mass, volume, and cost.

In the remainder of this paper, the design of several reconfigurable devices (i.e., two bandpass filters and a diplexer with three and two discrete states, respectively) is fully discussed. Additionally, the measured results of one of the filters and of the diplexer are also discussed in this paper. A very good agreement between the simulated data and the measured results is found, thus providing a very solid proof-of-concept for both the novel reconfigurable structures and their design procedure. Finally, a rigorous study of the corona and multipactor effects is also performed, with the aim of demonstrating that the devices we discuss can operate correctly under high-power microwave signals.

The content of this paper is organized as follows. Sec-

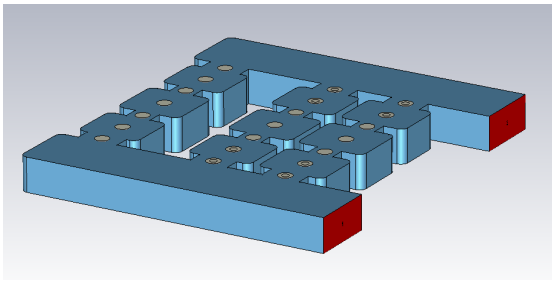

FIGURE 1. Reconfigurable rectangular waveguide filter structure for high-power applications.

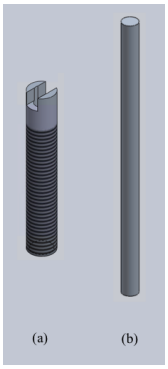

FIGURE 2. Modified Tuning Pins (MTPs): (a) Hollow M4 tuner used for a manual tuning of cavities and coupling windows; (b) Inner pin used to short circuit cavities or coupling windows by inserting it in the hollow M4 tuner.

tion II describes the topology of the reconfigurable filters. Section III details the specifications of the filters and outlines the design procedure. In section IV, we then discuss in detail the design procedure for the reconfigurable filters and the measured response of a prototype. In section V, we demonstrate the use of MTPs in a reconfigurable diplexer, providing also a detailed discussion of the design procedure, as well as the measured performance of a prototype. After that, a corona and multipaction analysis of both reconfigurable devices is performed in section VI. Section VII is devoted to outline the developments needed for the further commercial use of the proposed reconfigurable devices. The paper is concluded with a summary of the key achievements described in the paper.

II. RECONFIGURABLE WAVEGUIDE FILTER STRUCTURE

The structure that we propose to use to implement reconfigurable rectangular waveguide filters for high-power applications is shown in Fig. 1. The key enabling technology is the modified tuning pin (MTP) that was first introduced in [22]. For the sake of clarity, we now briefly describe how the MTPs operate. The MTPs can provide two different states, namely, ON and OFF (Fig. 2). The inner pin (Fig. 2 (b)) can be removed from the hollow M4 tuning element (Fig. 2 (a)) in order to obtain the ON state. To switch from the ON to the OFF state, the inner pin must be inserted until it makes contact with the bottom of the device. The hollow M4 tuners are adjusted manually to tune each filter cavity and coupling window, and also to compensate for eventual manufacturing inaccuracies. The M4 tuners are, therefore, adjusted only once.

It is important to note, at this point, that the reconfigurability is achieved using exclusively the inner pins of the MTPs. By removing and/or inserting specific inner pins, we can select the different filter states, thus completely modifying the performance of the filter both in terms of bandwidth and central frequency. Fig. 3 shows how to select each discrete channel by changing the position of the MTPs.

Before going any further, however, we believe that it is appropriate to clarify the difference between *tunable* and *reconfigurable* filters. In this context, therefore, we propose the following definition:

- A tunable filter is a device that includes tuning elements or screws that can be used to correct the effect of manufacturing errors, both in terms of center frequency and (or) bandwidth. The tuning range is normally limited to a few percent of the nominal value.
- A reconfigurable filter is a device that includes mechanical elements that allow to change significantly the filter behavior. Changes may affect the center frequency and (or) the bandwidth of the filter. The changes introduced, normally, go far beyond a few percentage points resulting in completely different filter performances (or states). Furthermore, reconfigurable filters may also include tuning elements to be used to compensate for manufacturing errors to obtain the desired performance in each of the separate states.

A key aspect of the solution that we propose is that it opens the possibility of remote, computer-controlled reconfiguration of the filters by lifting or lowering the central pin of the MTPs using a simple, low-cost linear actuator. The correct tuning of cavities and coupling irises is, in turn, assured by the M4 hollow tuner that is adjusted to the required penetration and permanently fastened to the filter body. As we will show in the reminder of this paper, once the tuners are adjusted, the filter can be reconfigured without the need of additional tuning.

However, it is important to note that, in this paper, we only provide the necessary basic proof-of-concept. The inclusion of computer-controlled linear actuators would require very significant additional work that goes, in our opinion, well beyond a proof-of-concept.

III. SPECIFICATIONS AND DESIGN PROCEDURE

Next, we will design two reconfigurable waveguide filters (namely, Filter A and Filter B). The input and output waveguide ports of the filters are implemented in WR-75 waveguide ($a = 19.05$ mm, $b = 9.525$ mm), and both filters have three discrete states and are of order three. The return loss of Filter A should be greater than 20 dB, while the return loss of Filter B should be better than 25 dB. The center frequencies

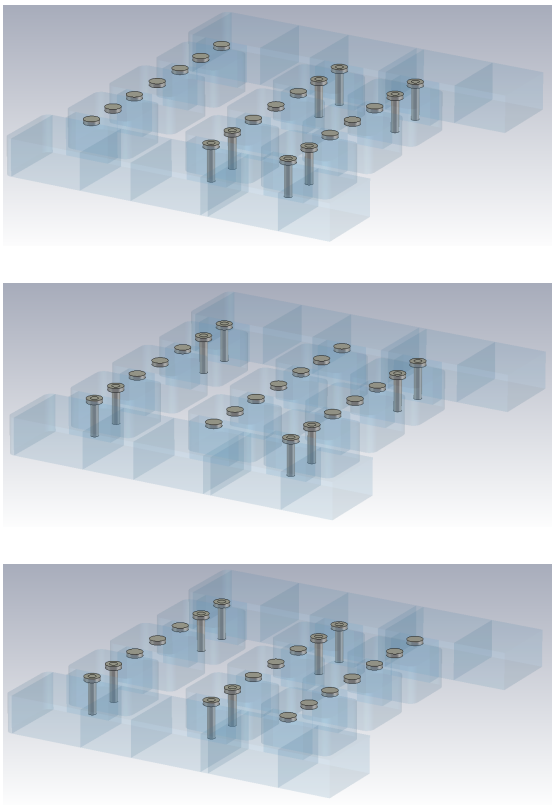

FIGURE 3. MTP configurations for selecting the different states: first (top), second (central) and third states (bottom).

TABLE 1. Filter A: center frequency and bandwidth for each discrete state.

State	*Center frequency* (GHz)	*Bandwidth* (MHz)
1	10.875	125
2	11.0	125
3	11.125	125

TABLE 2. Filter B: center frequency and bandwidth for each discrete state.

State	*Center frequency* (GHz)	*Bandwidth* (MHz)
1	11.0	62.5
2	11.0	125
3	11.0	250

and bandwidths of the three discrete states of the filters are collected in Table 1 (Filter A) and Table 2 (Filter B).

A standard milling technique will be used for manufacturing the body and cover of both filters. As a consequence, rounded corners (2 mm radius) must also be included in all the cavities. To simplify the process, we have split the design into two steps:

1) Step 1: A low accuracy (LA) model of the filter is obtained. This filter does not have cavities with rounded corners and does not include the M4 tuners.
2) Step 2: A high accuracy (HA) model of the filter is obtained. The HA filter will include all the features omitted in the previous step.

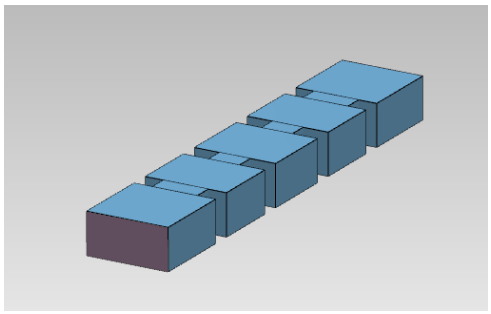

FIGURE 4. In-line filter channel.

For the first step, we have used the commercial simulator FEST3D from AuroraSat (now with Dassault Systèmes). The following set of computational parameters has been used (computationally fast, low accuracy model): 10 accessible modes, 30 basis functions and 300 terms for computing the Green's functions (a thorough description of these parameters can be found in [23]). The details of the design procedure are described in the next section. In any case, this step is particularly simple given the computational efficiency of the EM simulator FEST3D.

After designing the LA filter, we need to obtain the HA model of the filter including the features we omitted in the first step. For this stage of the design process, the full-wave software CST Microwave Studio has been used. Despite the fact that the HA simulations of the filter will need a substantially longer computation time, we can easily go from the LA to the HA model using the Aggressive Space Mapping (ASM) [24]–[27]. This is because, using the ASM technique, most of the simulations necessary to move from the LA to the HA space are carried out in the LA model.

It is important to note at this point that it is indeed true that the design of 3-pole in-line filters can be carried out with direct optimization without using ASM. However, we highlight in this paper the use of ASM because, using the approach we propose, the readers can indeed design significantly more complex reconfigurable structures that will strongly benefit from the use of ASM.

IV. RECONFIGURABLE FILTERS

In the following sections, we describe in detail the design process for Filter A and Filter B.

A. DESIGN OF FILTER A

First of all, the independent channel filters must be designed in the LA space. To do that, we use a filter model based on transmission lines and ideal inverters. This model provides us with the target Chebyshev response for each channel [13]. After that, the design procedure described in [28] is used to derive the in-line model of each filter (Fig. 4).

As we can see from Fig. 1, the length of all filter channels must be the same. In order to deal with this requirement, we have three possibilities:

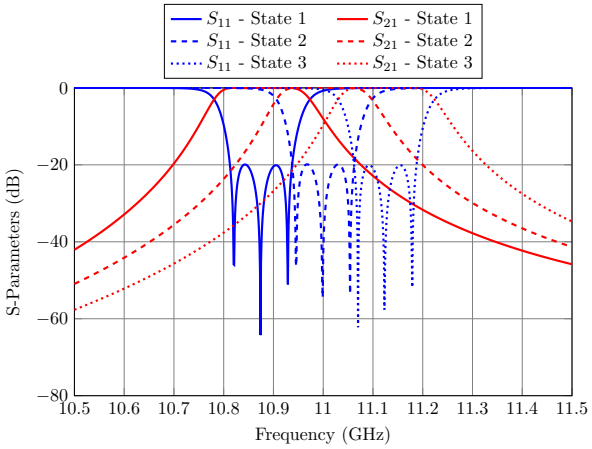

FIGURE 5. Electrical response of the separate filters. These filters represent the three states of the reconfigurable device.

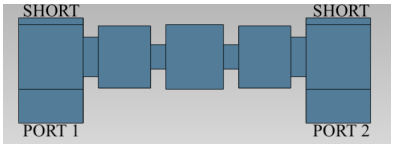

FIGURE 6. Step 1: The first filter is added to the manifold.

- As in [29], the filters can be coupled to the manifold by means of stubs whose dimensions can be afterwards optimized.
- The resonators length can be kept constant, while the resonators widths can be used as optimization parameters. This approach allows us to decrease the overall device footprint by coupling directly the channel filters to the manifold.
- The filters can be folded along their center to avoid completely this constraint [30].

However, since the scope of this paper is limited to providing a reconfigurability proof-of-concept, we have chosen the second option because of the inherent simplicity.

The performance of the three separate filters is shown in Fig. 5. Once the three independent filters (or states) have been designed, they can be added to the manifold by following these steps:

1) The first filter is added to the manifold (see Fig. 6). Then, the distance to the short circuit is optimized, as well as the widths of the first two elements of the filter (aperture and cavity). Please note that, as a general rule, our investigation indicates that the first filter (or channel) should be the one with the narrowest bandwidth, or the one with the highest frequency.
2) Once the first filter is designed, the state of the MTPs is changed to the OFF state. After that, the second filter is added to the manifold, as shown in Fig. 7 (top). It is important now to note that, after changing the state of the first filter MTPs, the central cavity of the filter (and the related adjacent apertures) will not affect the electrical response of the second filter (active channel). Therefore, some computation time can be saved if the central part of the first filter is not included in the simulations (see bottom of Fig. 7). As it was already mentioned in Section II, note that the entire MTP does not need to be simulated to short circuit the inactive channel. In fact, we only need to include in the simulations the (short circuiting) inner pin of the MTP.
3) The previous step is repeated until all the filters (channels) have been added to the manifold. In this particular design, the MTPs of the second filter are set in the OFF state and the third filter is added to the manifold, as in Fig. 8. The simulated data obtained after performing Steps 1, 2 and 3 are shown in fig. 9.
4) A further optimization of the first two states is required after assembling the whole reconfigurable device, since the active filter has been loaded by the filters added in Steps 2 and 3. The final electrical response that we have obtained is shown in Fig. 10.

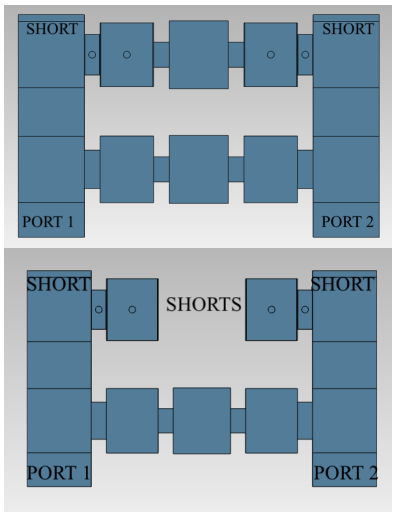

FIGURE 7. Complete (top) and reduced (bottom) structures after addressing Step 2 (note that both of them provide the same electrical response).

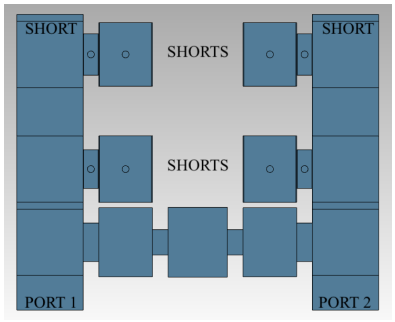

FIGURE 8. Step 3: The third channel (filter) is added to the manifold.

Once the filter has been designed in the LA space, the HA model shown in Fig. 1 can be easily obtained using any of the versions of the ASM technique [24], [26], [27]. The HA filter must include rounded corners in all cavities and also

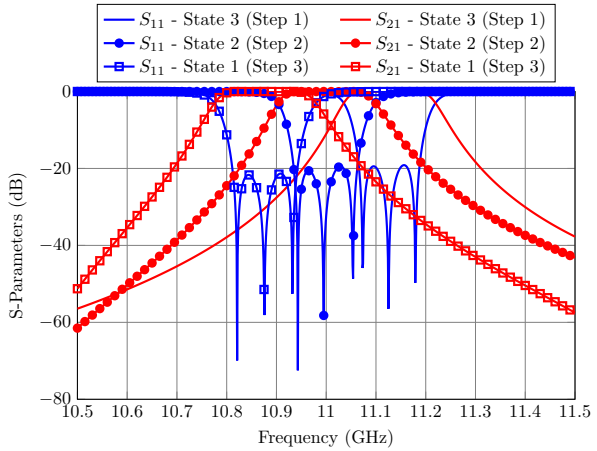

FIGURE 9. Filter performance after completing Steps 1, 2 and 3.

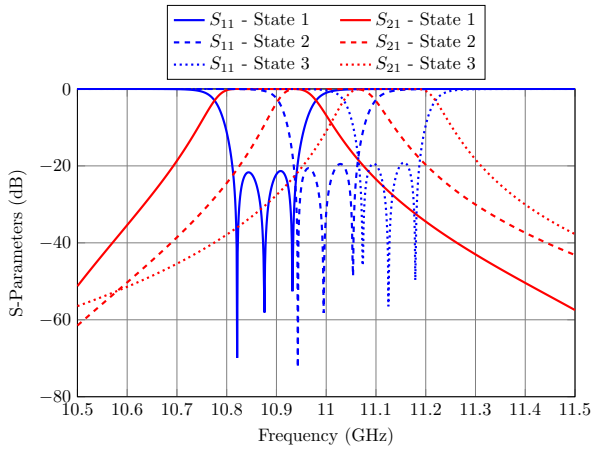

FIGURE 10. Performance of the LA filter. In order to change between the possible states, we must set the inner pins of the MTPs as shown in Fig. 3.

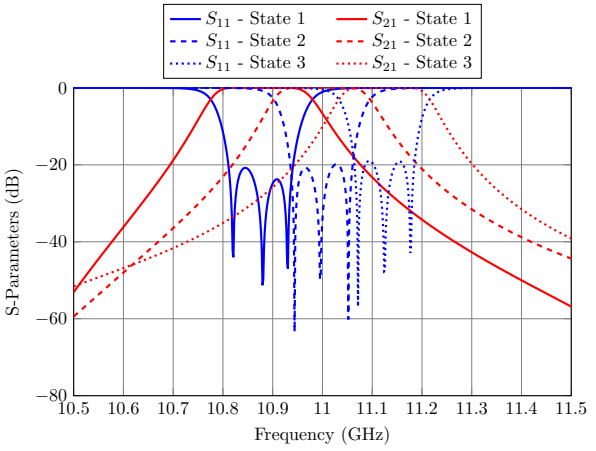

FIGURE 11. Electrical response of the HA filter.

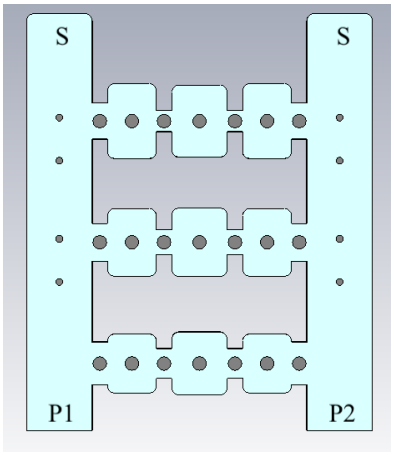

FIGURE 12. Filter B. Note that several removable shorting pins have been added to the manifold.

the hollow M4 tuners of the MTPs. The penetration of the tuners has been set at 1 mm to permit future bidirectional adjustments. After two ASM iterations per filter (where most simulations are performed in the LA space), the required specifications are finally met by the HA model of the filter, as we can see in Fig. 11.

Finally, it is interesting to note that, in the structure just discussed, the same manifold can be used in different states (while maintaining a good return loss level) since the input couplings are fully tunable. As a result, even if the manifold is not the perfect manifold for the given filter frequency and bandwidth, it is generally possible to recover the required return loss level by properly adjusting the input coupling and the manifold lengths at the same time. However, if we add more filters and the manifold becomes longer, it may not be possible to recover the correct performance. In the next section we describe a procedure that can be used to eliminate this restriction.

B. DESIGN OF FILTER B

In Filter A there was a limitation regarding the maximum states of the reconfigurable filter. The origin of this limitation is the *length* of the manifold. As we add new filters (or channels), the length of the manifold increases and thus, it becomes harder to optimize the structure. A straightforward way to overcome this limitation is to include a number of removable shorting pins in the manifold. The design of Filter B has been carried out using this procedure (see Fig. 12). Adding shorting pins to the manifold introduces two benefits:

- The first is that the separation between channels can be readily controlled. This is important because, since the filter will be fabricated in two parts (i.e., the body and cover) that we will assemble together using screws, if there is enough physical space between the channels it will be easier to include enough closing screws (see Fig. 13) so that the filter will have a better behavior in terms of losses. In this context, it is important to note that, following the method described in [12], the sections of waveguide between the channels should be about half

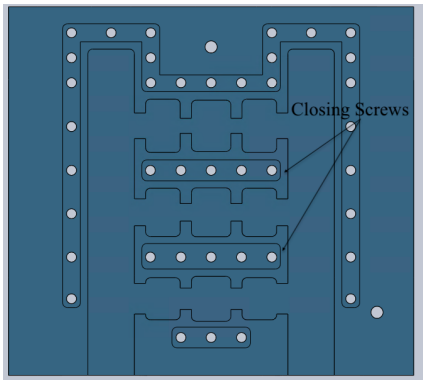

FIGURE 13. Closing screws of Filter B.

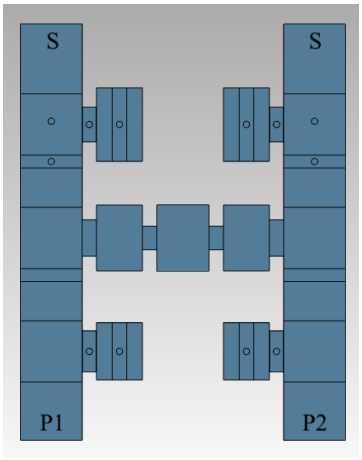

FIGURE 14. LA structure for Filter B (2nd state).

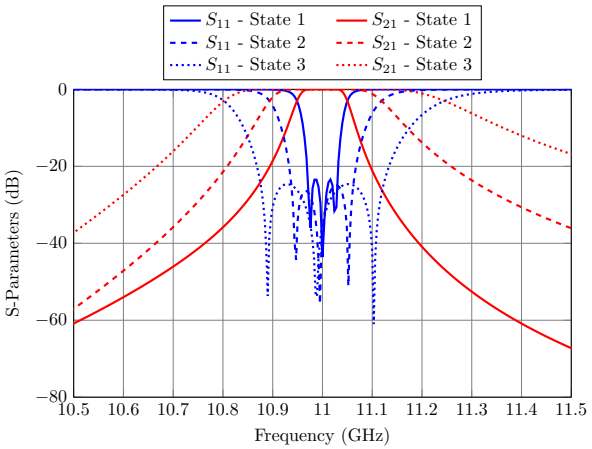

FIGURE 15. Filter B: electrical response of the LA model.

wavelength long. This distance is indeed sufficient to provide enough space for the closing screws. However, in our investigation we have found that, if we make the manifold too long, the optimization of the structure becomes problematic. We have, therefore, made an effort to keep the manifold as short as possible so that the structure becomes easier to optimize. To this end, additional shorting pins have been added to reduce the effective electrical length of the manifold.

- The second advantage is that the design becomes more modular, since the interaction between the channels is reduced due to the additional shorting pins. More specifically, each shorting pin effectively introduces two sections of below cutoff waveguide in parallel. This, in turn, reduces the power exchange (S_{12}) between the channels, thus strongly reducing the interactions.

The design of Filter B follows the same procedure as the one we described for filter A. The different filter channels are first designed, and then added progressively to the manifold. After that, the first two filters channels should be re-optimized, as we discussed in the design of Filter A. The LA filter structure for the second state is shown in Fig. 14 (as an example), while Fig. 15 shows the electrical response of the filter. After designing the LA structure, ASM is used for obtaining the HA model (see Fig. 12).

C. EXPERIMENTAL VALIDATION

As an experimental validation, we have manufactured Filter B in aluminum to validate both the proposed filter structure and the design procedure. Fig. 16 shows a photograph of the filter prototype, and Fig. 17 to Fig. 19 show the filter performance as compared to the simulated response. Although the agreement between the simulated and measured data is very good, we can observe that the measurements are affected by noise. Our investigations indicate that the source of the noise is the limited manufacturing accuracy of the MTPs used for this proof-of-concept. In any case, the agreement that we demonstrate between simulations and experimental data fully validates both the proposed topology and the design procedure.

Finally, it is important to note that the same filters could also be used to provide the same reconfigurability function using rotary switches instead of MTPs. However, the structure would require the same number of filters, two rotary switches and additional waveguide lengths to implement the connection between filters and switches. The result would be a very significant increase in mass, volume and cost. The use of the solution that we propose in this paper can, therefore, result in significant savings.

V. RECONFIGURABLE DIPLEXER

The use of the MTPs is not limited only to reconfigurable filters. In this section, the design of a high-power reconfigurable diplexer having two discrete states is addressed. The two discrete states of the device are shown in Fig. 20. Moreover, the specifications concerning the center frequencies and bandwidths of the two discrete states of the diplexer are shown in Table 3 (state 1) and Table 4 (state 2).

The input and output waveguide ports of the diplexer are implemented in WR-75 waveguide ($a = 19.05$ mm, $b = 9.525$

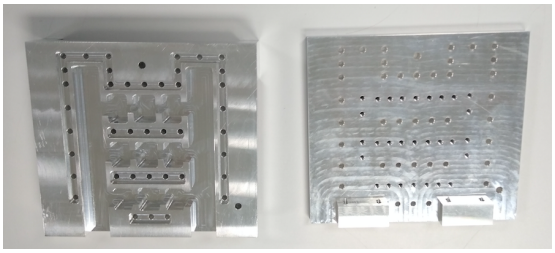

FIGURE 16. Filter B: photograph of the filter prototype. The breadboard has been fabricated in aluminum.

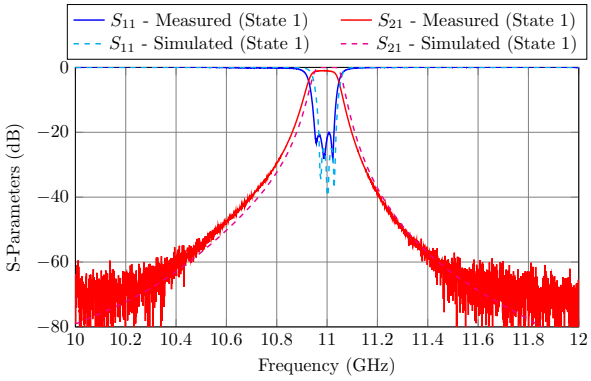

FIGURE 17. Experimental results compared to the HA model performance for the first state.

TABLE 3. Center frequencies and bandwidths for the state 1 of the reconfigurable diplexer.

Center frequency (GHz)	*Bandwidth* (MHz)
10.9075	125
11.155	250

mm). A minimum return loss of 25 dB is required, and the filters of the diplexer are of order $N=5$.

According to [13], a diplexer is defined as contiguous when the channel separation (assuming all channels share the same bandwidth) is below $0.25 \times BW$. Therefore, the central

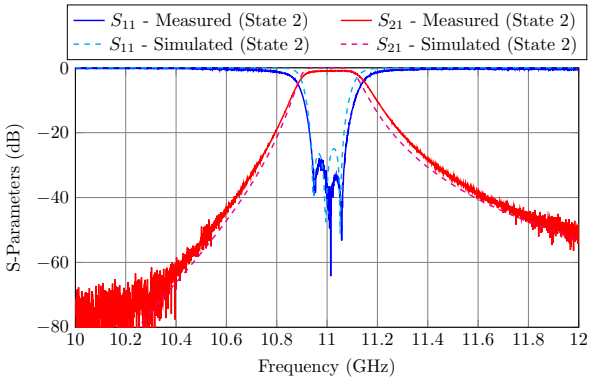

FIGURE 18. Experimental results compared to the HA model performance for the second state.

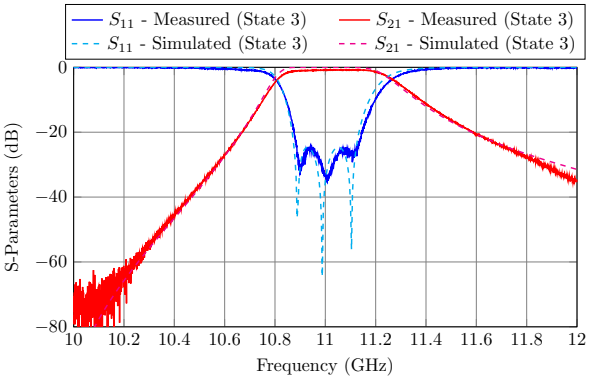

FIGURE 19. Experimental results compared to the HA model performance for the third state.

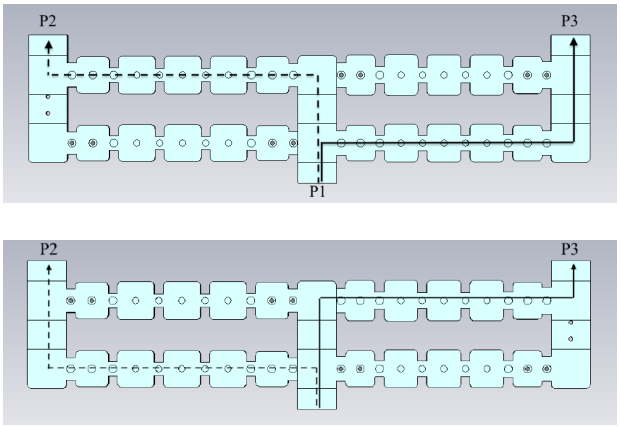

FIGURE 20. Topology of the proposed reconfigurable diplexer for high-power applications. Top: State 1. The two paths of the signal for the first state have been drawn. Bottom: State 2.

TABLE 4. Center frequencies and bandwidths for the state 2 of the reconfigurable diplexer.

Center frequency (GHz)	*Bandwidth* (MHz)
10.845	250
11.0925	125

frequencies have been chosen to ensure that the channels are separated by 60 MHz ($\approx 250 \times 0.25$). It is important to note, at this point, that the frequency plan of the diplexer has been designed to be compliant with the principles of the current frequency allocation strategy for communication satellites [31]. More specifically, the available spectrum is divided in a number of frequency bands. Normally speaking, two contiguous bands are allocated to each satellite communication system. The lower frequency band is normally used for transmission from the satellite, while the higher band is used for the reception of the signals from the ground stations. In this context, therefore, our diplexer specifications are aimed at maintaining the same transition from the transmit to the receive band, while reconfiguring the actual transmit and receive channel bandwidth. To our knowledge,

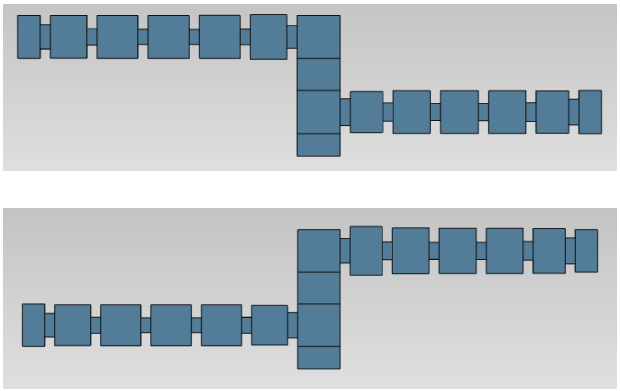

FIGURE 21. Isolated diplexers whose electrical response provides the first (top) and second (bottom) states of the reconfigurable diplexer.

this type of reconfiguration has not been demonstrated, so far, in the technical literature. This is, therefore, an additional innovative contribution of this paper.

The design procedure is again split in two steps. First, the LA model of the diplexer is designed. After that, the ASM is used to produce the HA model. The simulation setup is the same as in Section III.

A. DESIGN PROCESS IN THE LOW-ACCURACY SPACE

Next, the design process of the LA model of the diplexer is discussed.

1) The first step is to obtain the isolated diplexer associated to each state. The combination of the manifold diplexers shown in Fig. 21 provides us with the reconfigurable diplexer. In order to design these diplexers, we can follow the design guidelines outlined in [13], [32]. In this stage of the design process, both the cavities and coupling windows widths will be optimized. The electrical response of the independent diplexers are shown in Fig. 22.
2) Next, the isolated diplexers are combined in a four-port component, as we show in the top of Fig. 23. For each state, it will be necessary to perform a slight optimization of the dimensions of the first coupling window and cavity of each section with the aim of recovering the responses of the independent diplexers. It is interesting to note that we can carry out the necessary optimizations using the complete component (top of Fig. 23) or using a reduced structure (bottom of Fig. 23). This is because, due to the MTP, the full and reduced structures have the same response. In fact, the reduced model has been used in this case to accelerate the design procedure. The optimized responses shown in Fig. 24 have been finally obtained.
3) The next step consists of combining the common outputs of the branches. To this end, we proceed as follows:
    a) Before the independent diplexers are designed, the initial channels are added to the manifold.

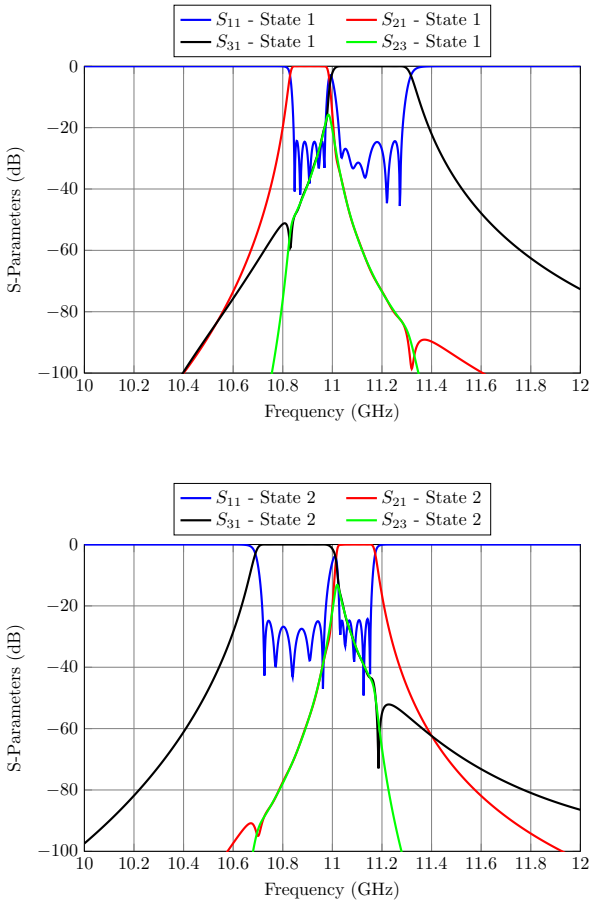

FIGURE 22. Electrical response of the independent diplexers: state 1 (top) and state 2 (bottom).

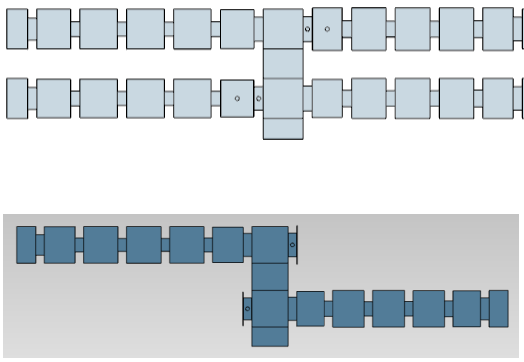

FIGURE 23. The isolated filters are combined considering the whole diplexer (top) or a reduced structure (bottom).

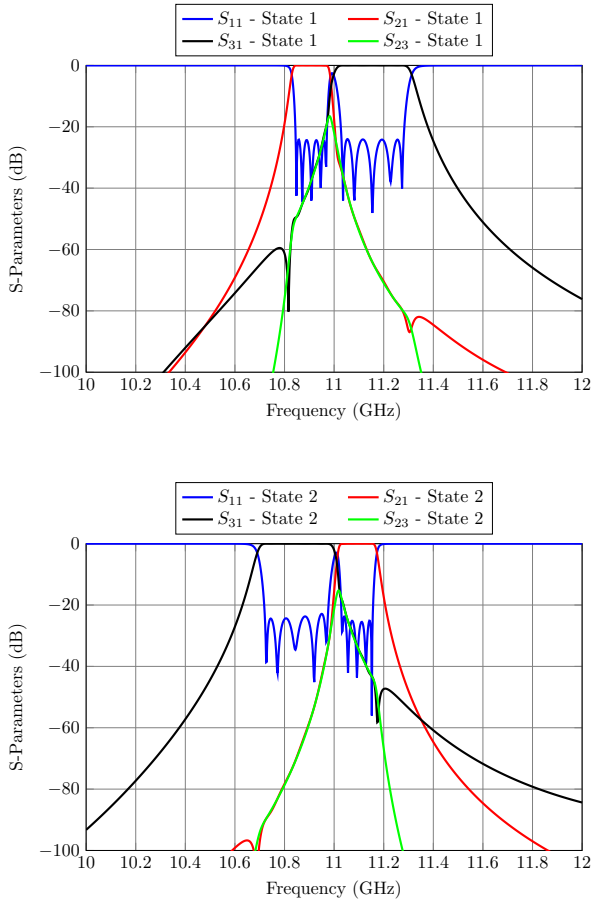

FIGURE 24. Electrical response of the four-port component: state 1 (top) and state 2 (bottom).

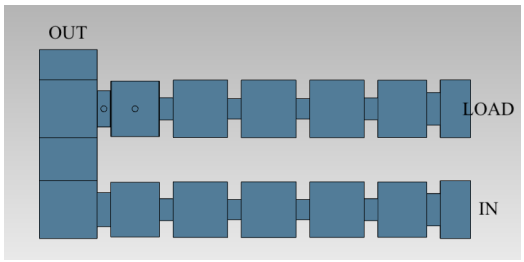

FIGURE 25. Addition of the initial channels to the manifold.

The MTPs of one filter are switched to the OFF state, as shown in Fig. 25. Afterwards, the first coupling window and cavity of the active filter (these are the closest elements to the manifold) are optimized with the aim of recovering the response of the ideal filter (Fig. 26).

b) Then, the manifold is short-circuited by inserting a pin and the state of the MTPs is switched, as shown in Fig. 27. Next, the pin position is optimized, as well as the dimensions of the active filter elements closer to the manifold. The response shown in Fig. 28 is obtained after this optimization process.

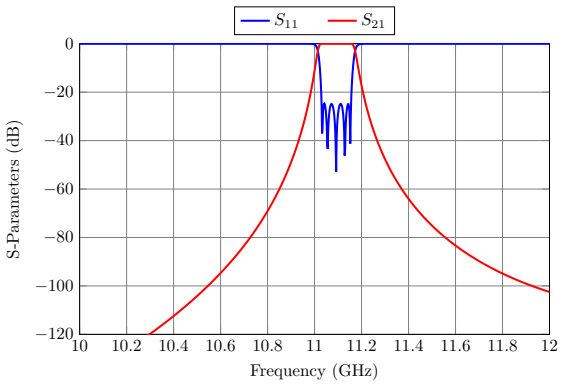

FIGURE 26. Response of the component displayed in Fig. 25 after optimizing some elements of the active filter.

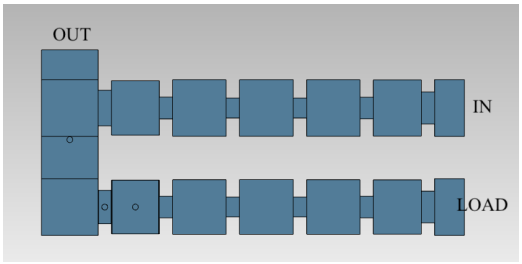

FIGURE 27. Combination of the common outputs of the branches.

From the simulated results, we can now see that, around 11.8 GHz, there is a peak in the S_{21} parameter resembling a transmission zero. The origin of this undesired peak lies in the fact that the pin we inserted in the manifold is behaving as an inductive post and, therefore, it is creating a new resonator between the pin and the manifold short circuit. In fact, as shown in Fig. 29, the resonant frequency of the second mode of this resonator is equal to 11.8 GHz.

With the aim of eliminating this unexpected reso-

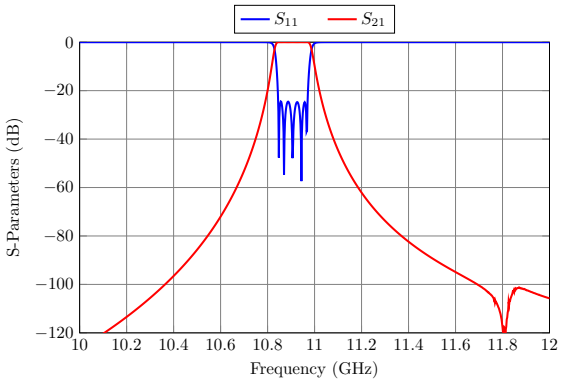

FIGURE 28. Response of the component displayed in Fig. 27 after the optimization.

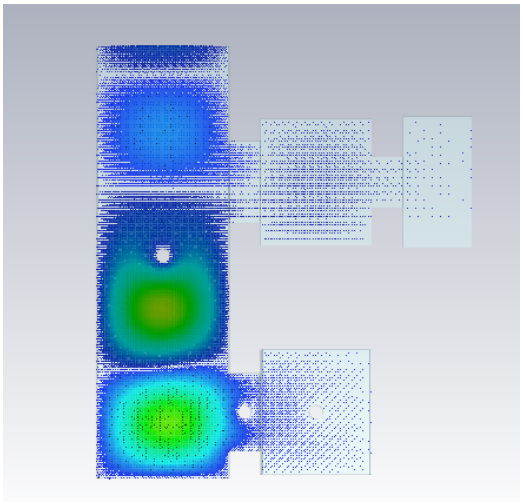

FIGURE 29. Electric field of the structure shown in Fig. 27 calculated at $f = 11.8$ GHz.

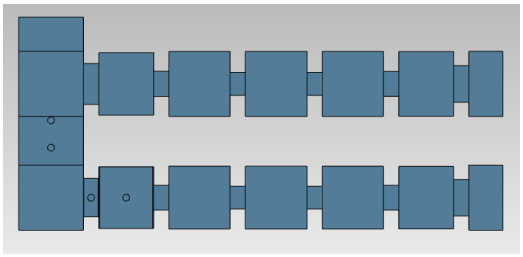

FIGURE 30. A new pin is inserted in the manifold to eliminate the undesired resonance.

nance, we propose to introduce another pin in the manifold (see Fig. 30) to move the peak out of the operation band of the device. It is important to note that, after inserting this pin, the new resonant frequencies of the manifold are 9.62 and 14 GHz, and, as a consequence, the undesired peak is no longer present, as we can see in Fig. 31.

4) Finally, half of the structures described in the second and third steps, are combined. The low precision models of the reconfigurable diplexer for the first and second states are shown in Fig. 32, while their electrical responses are shown in Fig. 33.

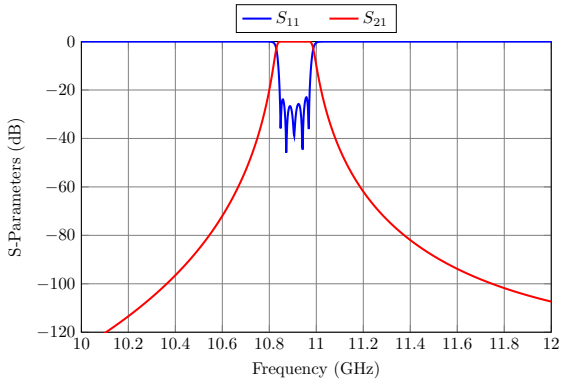

FIGURE 31. Response of the component displayed in Fig. 30.

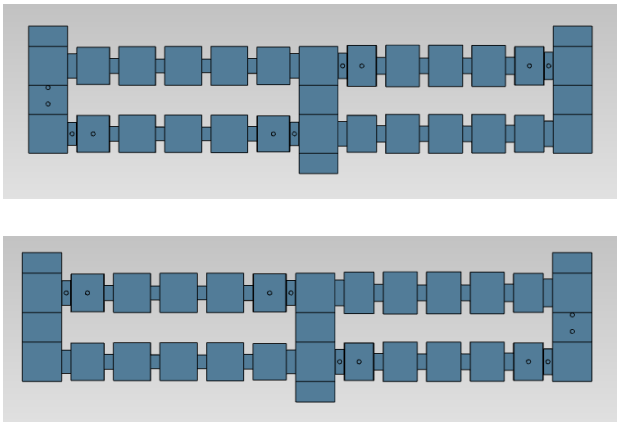

FIGURE 32. LA models for the first (top) and second (bottom) states of the designed diplexer.

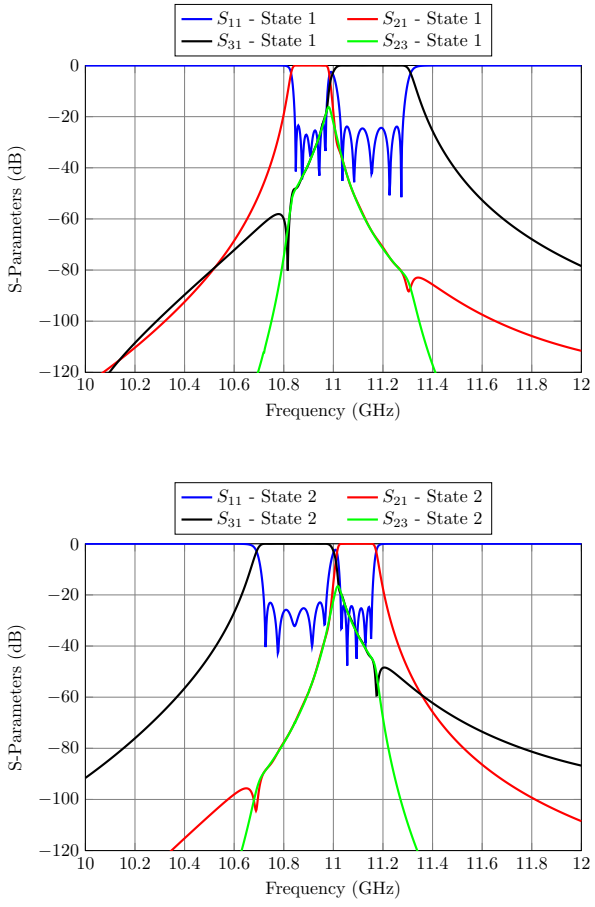

FIGURE 33. Electrical response of the low precision diplexer shown in Fig. 32 for the first (top) and second (bottom) states.

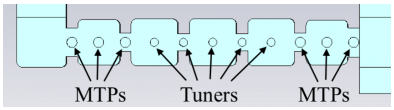

FIGURE 34. The HA model includes rounded corners, MTPs and commercial tuners.

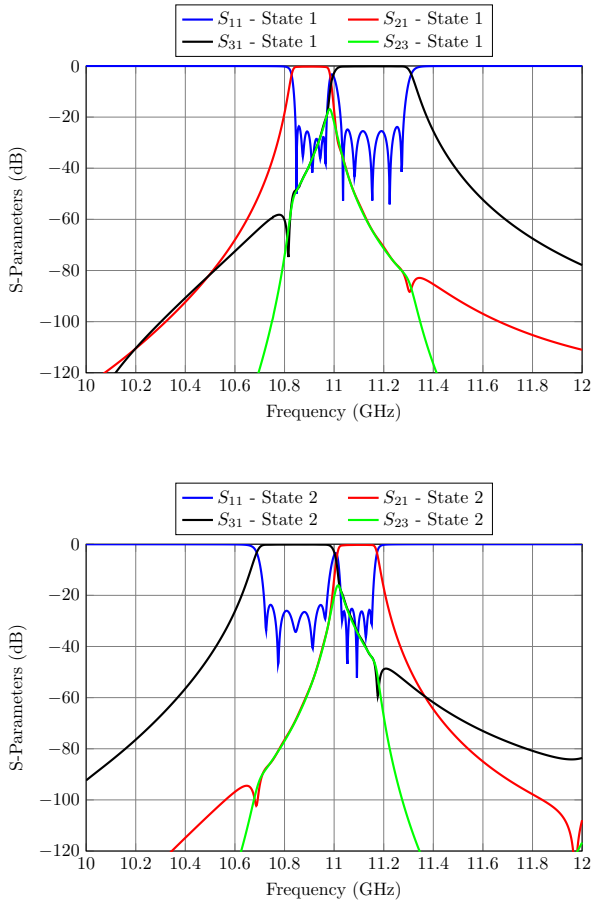

FIGURE 35. Responses of the first (top) and second (bottom) states of the diplexer in the HA space.

B. DESIGN OF THE DIPLEXER IN THE HIGH-ACCURACY SPACE

After designing the diplexer in the low-accuracy space, the ASM technique [27] can be used to obtain the corresponding structure in the high-accuracy (HA) space. This HA model must include rounded corners in the resonators, the MTPs, and the presence of the M4 tuners (see Fig. 20).

As already discussed in Section IV, the MTPs do not have to be included in all resonators and coupling windows. Using a number of commercial gold-plated tuners of radius 1.6 mm, as shown in Fig. 34, will improve the behavior of the diplexer in terms of losses.

We have only needed 3 iterations in the ASM procedure to obtain the response shown in Fig. 35.

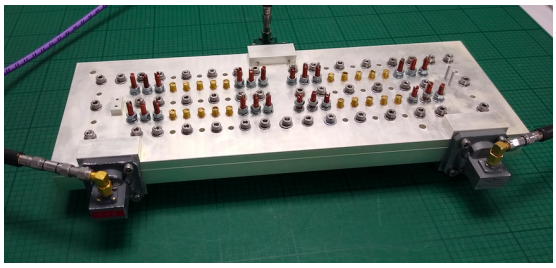

FIGURE 36. Assembled reconfigurable diplexer.

C. PRACTICAL IMPLEMENTATION OF THE DIPLEXER

With the aim of validating the design procedure, a diplexer prototype has been fabricated (in aluminum) and measured. A photograph of the assembled component is shown in Fig. 36, where a standard WR-75 waveguide is used to feed the device.

Fig. 37 shows the comparison between simulations and measurements for the two states. A very good agreement is observed between the simulated data and the experimental results.

Although an equiripple response has not been recovered for the state 2 (due to manufacturing accuracy), it is important to note that the return loss is greater than 23 dB and that all lobes of the S_{11} parameters are present in the response. Furthermore, the filters with the narrower bandwidth exhibit losses of 1.3 dB (state 1) and 1.2 dB (state 2), while the losses of the filters with the wider bandwidth are of 0.8 dB (state 1) and 1.0 dB (state 2). The results obtained do provide, therefore, a very solid proof-of-concept for both the topology and the design process that we have used for the reconfigurable diplexer.

Finally, it is important to mention that an identical reconfigurable diplexer function could also be implemented using rotary switches instead of MTPs. However, the structure would require the same number of filters, three rotary switches, and additional waveguide lengths to implement the connection between filters and switches. The result would be a device exhibiting a significant increase in terms of mass, volume and cost with respect to our solution based on the use of MTPs.

VI. HIGH-POWER ANALYSIS

The ability of operating correctly under high-power signals is a key requirement for all components used in the output networks of many microwave payloads that require significant output power levels, for both space and ground applications. A mandatory first step to verify the correct operation of the devices is to carry out a high-power analysis, in particular with respect to multipactor and corona effects [33], [34]. We have, therefore, carried out a number of simulations in order to identify the power (Watts) and pressure (mbar) where the multipactor and corona effects can be initiated in the reconfigurable devices described in this paper (in particular, we have analyzed filter B and the diplexer). As we report below, the

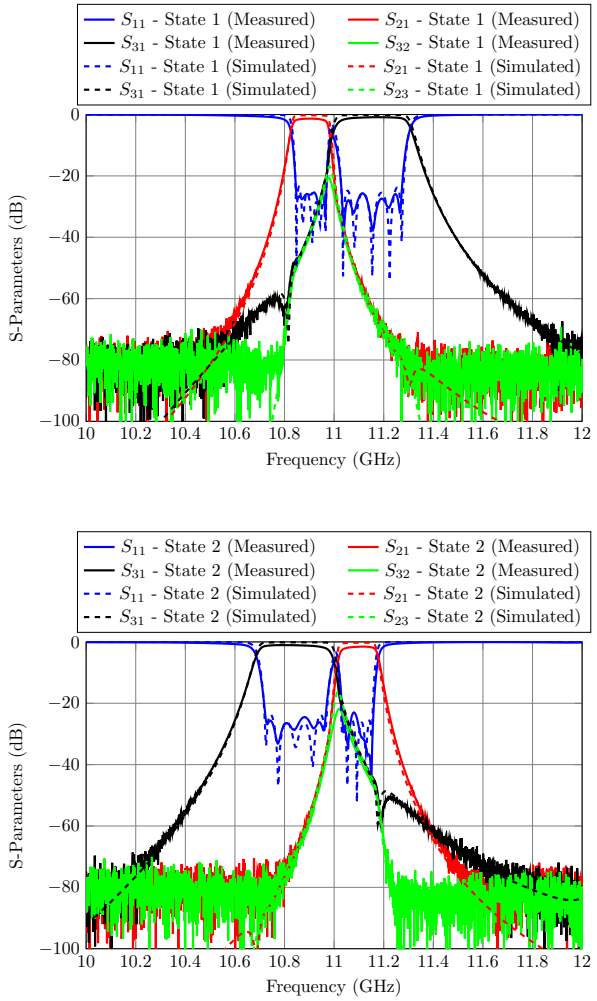

FIGURE 37. Experimental results for the state 1 (top) and state 2 (bottom) of the designed diplexer.

results obtained clearly confirm that both components can be used in high-power applications.

It is important to note, at this point, that only the results regarding state 1 of the reconfigurable filter B will be presented in this section. This is because this state is the one with the smaller bandwidth (see Table 2), thus resulting in the lowest multipactor power threshold. Similarly, after analyzing the high-power phenomena in both states of the reconfigurable diplexer, we have concluded that state 1 is the one giving the lowest multipactor power threshold. As a consequence, also for the diplexer, we discuss only state 1.

In order to perform the simulations, we have first identified the maximums of the electric field intensity in the structures. For the reconfigurable filter B, the simulations have been performed at the frequencies where the group delay shows a maximum (f_1 and f_3), and also at the center frequency f_2 of the passband (see Table 2). For the reconfigurable diplexer, the simulations have been carried out at the maximum of the group delay of the electrical response (f_1, f_3 and f_5) and at the center frequencies f_2 and f_4 (see Table 3).

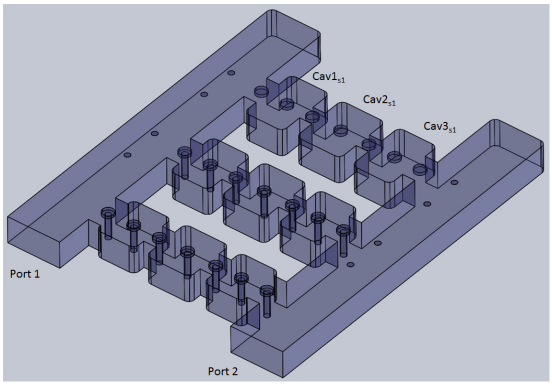

FIGURE 38. Structure for the state 1 of reconfigurable filter B.

The high-power simulations have been carried out using SPARK3D, while CST has been used for obtaining the EM fields. For multipactor prediction, the following set of parameters has been used:

1) Initial power: 1000 W
2) Maximum power: 1 MW
3) Growth factor of the power: 10^2
4) Frequencies of simulation: f_1, f_2 and f_3 (reconfigurable filter) and f_1, f_2, f_3, f_4 and f_5 (diplexer)
5) Initial number of electrons: 10000

Once we have identified the regions where the maximum of the electrical field is located (the regions of the structure where the multipactor effect is initiated), we have proceeded to identify the power (Watts) and the pressure (mbar) where the corona effect can be initiated. For corona predictions, the following set of parameters has been used:

1) Gas: Dry air
2) Temperature: 293 °K
3) Initial power: 100 W
4) Frequencies of simulation: f_1, f_2 and f_3 (reconfigurable filter) and f_1, f_2, f_3, f_4 and f_5 (diplexer)

A. RECONFIGURABLE FILTER

First, we have studied the reconfigurable filter B designed in section IV-B. Fig. 38 shows the structure for the state 1 of the device, where we have numbered the cavities for the sake of clarity. The maximums of the electric field intensity are located in cavities $Cav1_{s1}$, $Cav2_{s1}$ and $Cav3_{s1}$. Table 5 reports the multipactor power thresholds (in W) that we have obtained. As expected, the first cavity ($Cav1_{s1}$) shows the lowest threshold at $f = 11.044$ GHz with 8312 W. In addition, we show in Fig. 39 the multipactor results obtained for each simulation in this first cavity ($Cav1_{s1}$), evaluated at $f = 11.044$ GHz.

Next, we have studied the corona effect in the first cavity ($Cav1_{s1}$) of the reconfigurable filter (state 1). Table 6 shows the pressure (in mbar) and the power thresholds (in W) that we have obtained. The lowest power threshold is obtained at $f = 11.044$ GHz with 12.84 W and a pressure of 10 mbar. Finally, Fig. 40 shows the values obtained for each simulation

TABLE 5. Multipaction analysis for the state 1 of the reconfigurable filter B.

Frequency (GHz)	$f_1 = 10.960$	$f_2 = 11.0$	$f_3 = 11.044$
Structure	Multipactor power threshold (W)		
$Cav1_{s1}$	8752	13472	8312
$Cav2_{s1}$	9382	13564	8342
$Cav3_{s1}$	9500	13487	8625

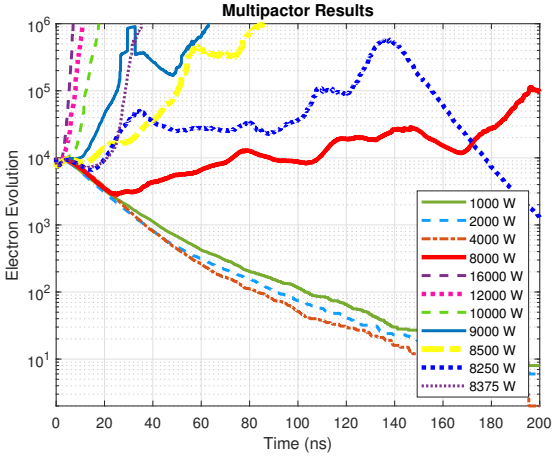

FIGURE 39. Multipactor simulation with discharges for the first cavity $Cav1_{s1}$ of the filter at $f = 11.044$ GHz.

TABLE 6. Corona analysis for the state 1 of the reconfigurable filter B (cavity $Cav1_{s1}$).

Frequency (GHz)	$f_1 = 10.960$	$f_2 = 11.0$	$f_3 = 11.044$
Pressure (mbar)	Power of the structure (W)		
1.00	80.44	118.09	63.56
2.15	39.87	58.51	31.48
4.64	22.50	32.97	17.91
10.00	16.30	23.89	12.84
21.54	18.99	27.74	14.85
46.42	40.48	59.01	31.51
100.00	116.42	168.965	89.87
215.44	337.03	488.87	259.90
464.16	1003.73	1455.89	773.97
1000	3319.50	4814.89	2559.71

(Paschen curves) in cavity $Cav1_{s1}$. In conclusion, the results that we have obtained clearly confirm that the reconfigurable filter structure we discussed is, indeed, appropriate for high-power applications, for both ground and space application. The only exception is in the higher atmosphere, where the pressure is significantly lower than the ambient pressure. However, this is not a limitation since, normally, high-power space payloads are activated only once the spacecrafts are in vacuum. On the other hand, if high-power operations are required in the transition region between earth and space, enclosure of the reconfigurable filter in a pressurized environment will ensure proper operations.

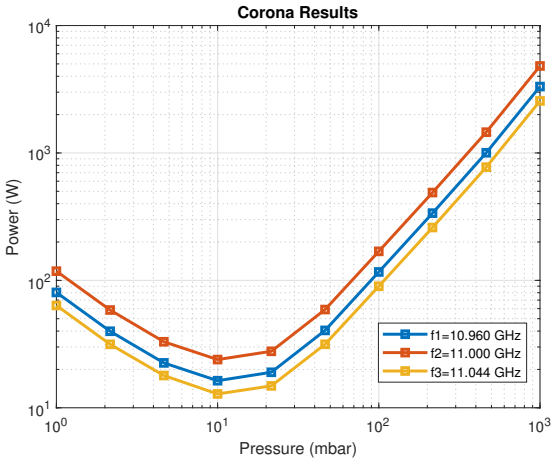

FIGURE 40. Corona simulation (dry air) for the first cavity ($Cav1_{s1}$) of the filter at $f = 10.960$, $f = 11.0$ and $f = 11.044$ GHz.

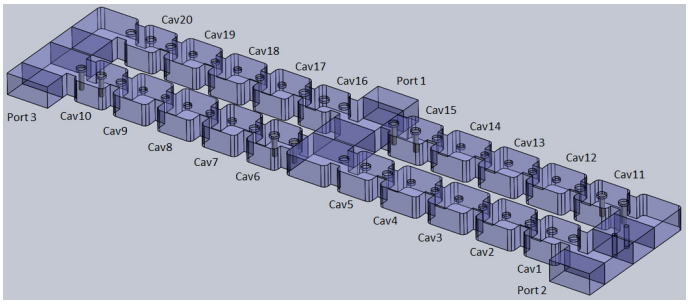

FIGURE 41. Structure for the state 1 of the reconfigurable diplexer.

B. RECONFIGURABLE DIPLEXER

Next, we have performed a high-power analysis of the reconfigurable diplexer (state 1) designed in section V. Fig. 41 shows the topology of this component, where we have numbered the different cavities for the sake of clarity. After computing the EM fields in the structure, we have observed that the maximum of the electrical field is located in the cavities labeled $Cav2$, $Cav3$, $Cav4$, $Cav18$, $Cav19$ and $Cav20$.

Table 7 reports the multipactor power thresholds (in W) obtained after performing the corresponding high-power simulations. The cavity $Cav4$ exhibits the lowest power threshold at $f = 10.982$ GHz with 5812 W. Additionally, Fig. 42 shows the evolution of the electron population in this cavity ($Cav4$) for different values of the input power, evaluated at $f = 10.982$ GHz.

Next, we have studied the corona effect in the cavity $Cav4$. Table 8 shows the pressure (in mbar) and the power thresholds (in W) that we have obtained. Cavity $Cav4$ presents the lowest power threshold at 10.832 GHz with 7.32 W and a pressure of 10 mbar. Finally, in Fig. 43 we show the values obtained for each simulation (Paschen curves) in this fourth cavity ($Cav4$).

Once again, the results obtained clearly confirm that the reconfigurable diplexer we proposed can be used with high-

TABLE 7. Multipaction analysis for the state 1 of the diplexer.

Frequency (GHz)	f_1 10.832	f_2 10.910	f_3 10.982	f_4 11.154	f_5 11.304
Structure	Multipactor power threshold (W)				
$Cav2$	6562	17750	5841	30750	13255
$Cav3$	5937	17825	5937	31250	13874
$Cav4$	7062	18252	5812	32122	16124
$Cav18$	6722	16922	5872	34749	13792
$Cav19$	7625	16620	7562	31435	13562
$Cav20$	6562	16850	6562	32782	13642

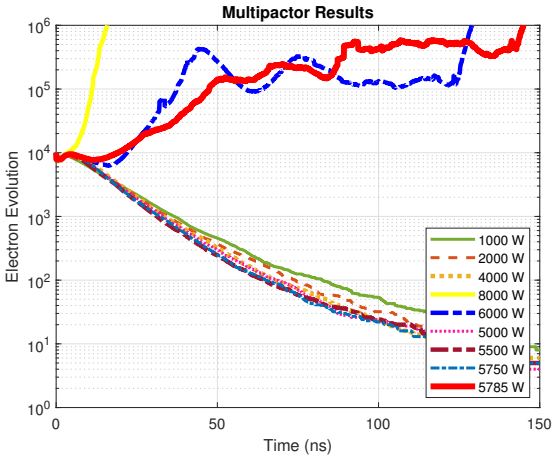

FIGURE 42. Multipactor simulation with discharges for the diplexer cavity $Cav4$ at $f = 10.982$ GHz.

TABLE 8. Corona analysis for the state 1 of the diplexer.

Frequency (GHz)	f_1 10.832	f_2 10.910	f_3 10.982	f_4 11.154	f_5 11.304
Pressure (mbar)	Power of the structure (W) Cav4				
1.00	35.69	104.63	39.33	$44.24{\cdot}10^3$	$872.84{\cdot}10^3$
2.15	17.82	52.21	19.62	$22.06{\cdot}10^3$	$439.11{\cdot}10^3$
4.64	10.18	29.80	11.18	$12.55{\cdot}10^3$	$248.82{\cdot}10^3$
10.00	7.32	21.35	7.99	8917	$176.37{\cdot}10^3$
21.54	8.51	24.69	9.19	$10.11{\cdot}10^3$	$197.92{\cdot}10^3$
46.42	17.75	51.26	19.0	$20.64{\cdot}10^3$	$404.91{\cdot}10^3$
100.00	49.16	141.80	52.61	$57.36{\cdot}10^3$	$1.09{\cdot}10^6$
215.44	137.90	397.61	147.51	$164.85{\cdot}10^3$	$3.19{\cdot}10^6$
464.16	426.03	1228.26	455.85	$506.16{\cdot}10^3$	$10.13{\cdot}10^6$
1000	1419.83	4093.39	1518.54	$1.69{\cdot}10^6$	$33.61{\cdot}10^6$

power microwave signals for both ground and space applications. Again, as expected, the only exception is the transition between earth and space. As already discussed, if necessary, a pressurized environment will eliminate any problems.

VII. FURTHER DEVELOPMENTS

As already discussed, the objective of this paper is to give a solid proof-of-concept for a possible implementation of

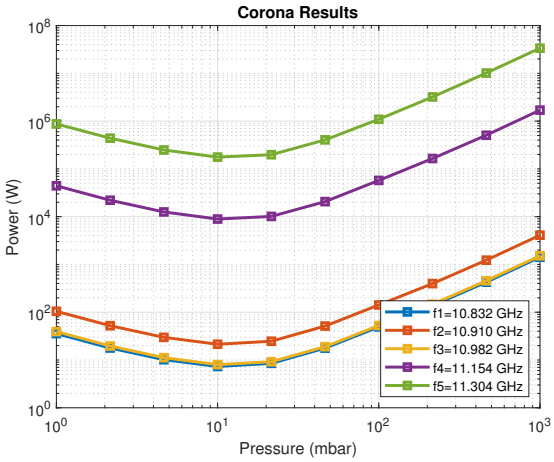

FIGURE 43. Corona simulation (dry air) for the cavity $Cav4$ of the diplexer, at $f = 10.832$, $f = 10.910$, $f = 10.982$, $f = 11.154$ and $f = 11.304$ GHz.

reconfigurable filters and diplexers in rectangular waveguide. The agreement demonstrated between simulations and measurement clearly indicates that this objective has been achieved. However, it is important to appreciate that, in terms of Technology Readiness Levels [1] (TRLs), the level reached with a proof-of-concept is TRL3. On the other hand, a commercial product is considered fully reliable when it reaches TRL9. It is therefore clear that a number of further development activities are required before the concept described in this paper can become a commercial product. However, it is important to note that this situation is indeed common in the initial stages of the development of any new product. In this context, therefore, we find it appropriate to outline in this section the main development activities that are required, in our opinion, to finally obtain a commercial implementation.

The first consideration is that the basic filter structures in rectangular waveguide, including the M4 tuners, are very frequently used in practical applications for both ground and space applications and, therefore, in our opinion, do not pose any basic industrialization problem, even for more complex rectangular waveguide filters that use cross couplings. This is also true both in terms of possible bandwidths and/or center frequency, and power.

The key element that needs further development is then the MTP in Fig. 2. As already discussed, the MTP is composed of two parts, a shorting pin and a hollow tuner. It is important to note that the shorting pins are not present inside the filters when the filters themselves are active. As a consequence, they have no effect on the filter performance. When the filters are deactivated by the shorting pins, as demonstrated during the design process, they have no electrical effect on the active filters. Furthermore, metallic tuners are very commonly used in many types of microwave filters. Our choice of an M4 tuner was dictated by the mechanical facilities at our disposal.

[1] https://en.wikipedia.org/wiki/Technology readiness level

However, a different size could also be used. What remains is, therefore, the shorting pin and the actuation mechanism.

In this context, what is important is to ensure the proper electrical contact between the pin and the bottom of the waveguide, including life-time and power requirements. However, the further developments required are, in our opinion, beyond the scope of this initial paper. In any case, this problem is similar to the one encountered in many commercial RF switches. We, therefore, believe that a viable practical solution can indeed be developed in the future.

VIII. CONCLUSION

In this contribution, we have discussed the proof-of-concept of how the recently developed modified tuning pins (MTPs) can be effectively extended to the development of a new family of reconfigurable filters and diplexers suitable for high-power applications. We have, in fact, demonstrated that several reconfigurable devices with a variety of discrete states, that are completely different from each other, can be readily designed using a simple step-by-step procedure.

In addition to theory, the proof-of-concept has been validated by manufacturing a filter with 3 states, and a reconfigurable diplexer with 2 discrete states. In all cases, excellent agreement has been found between the simulated and the measured data, thus fully validating both the topologies proposed and the corresponding design procedures.

Furthermore, the high-power behavior of the components that we have discussed has been analyzed in detail, showing that their performance in terms of corona and multipactor effects is fully adequate for both ground and space high-power operation.

In addition, it is important to note that, even though simple in-line filters have been used for this proof-of-concept, folded filters including cross-couplings to implement transmission zeros can be also used.

Finally, it is important to mention that, the reconfigurable structures that we have discussed, open the possibility of remote operation. This is because the MTPs inner pin does not need high-precision mechanisms to be displaced (in fact, a simple linear actuator could be used to this end). This aspect, in our opinion, makes the solution that we have proposed particularly attractive for the implementation of reconfigurable high-power output networks for both ground and space application.

REFERENCES

[1] E. Laplanche, N. Delhote, A. Périgaud, O. Tantot, S. Verdeyme, S. Bila, D. Pacaud, and L. Carpentier, "Tunable filtering devices in satellite payloads: A review of recent advanced fabrication technologies and designs of tunable cavity filters and multiplexers using mechanical actuation," *IEEE Microw. Mag.*, vol. 21, no. 3, pp. 69–83, 2020.

[2] U. Rosenberg, R. Beyer, P. Krauß, T. Sieverding, P. M. Iglesias, and C. Ernst, "Remote controlled high-Q cavity filters providing center frequency and bandwidth re-allocation," in *Proc. IEEE MTT-S Int. Microw. Workshop Series Adv. Mater. Processes for RF and THz Appl. (IMWS-AMP)*, 2017, pp. 1–3.

[3] U. Rosenberg, R. Beyer, P. Krauß, T. Sieverding, A. Papanastasiou, M. Pueyo-Tolosa, P. M. Iglesias, and C. Ernst, "Reconfigurable doublet dual-mode cavity filter designs providing remote controlled center frequency and bandwidth re-allocation," in *Proc. 46th Eur. Microw. Conf. (EuMC)*, 2016, pp. 532–535.

[4] U. Rosenberg, R. Beyer, P. Krauß, T. Sieverding, P. M. Iglesias, and C. Ernst, "Omux approach providing re-configuration of contiguous/non-contiguous channel allocations with variable frequencies and bandwidths," in *Proc. 46th Eur. Microw. Conf. (EuMC)*, 2016, pp. 536–539.

[5] J. Ossorio, J. Vague, V. E. Boria, and M. Guglielmi, "Exploring the tuning range of channel filters for satellite applications using electromagnetic-based computer aided design tools," *IEEE Trans. Microw. Theory Techn.*, vol. 66, no. 2, pp. 717–725, 2018.

[6] J. Ossorio, V. E. Boria, and M. Guglielmi, "Dielectric tuning screws for microwave filters applications," in *IEEE MTT-S Int. Microw. Symp. Dig.*, 2018, pp. 1253–1256.

[7] D.-S. Wu, Y. C. Li, Q. Xue, and B.-J. Hu, "Balanced dielectric resonator filters with multiple reconfigurable passbands," *IEEE Trans. Microw. Theory Techn.*, vol. 70, no. 1, pp. 180–189, 2022.

[8] C. Roy, W. Lin, and K. Wu, "Swarm intelligence-homotopy hybrid optimization-based ANN model for tunable bandpass filter," *IEEE Trans. Microw. Theory Techn.*, pp. 1–15, 2023 (early access).

[9] W. Lin, K. Zhou, and K. Wu, "Band-reconfigurable tunable bandpass filters based on mode-switching concept," *IEEE Trans. Microw. Theory Techn.*, pp. 1–11, 2022 (early access).

[10] Y. Xie, F.-C. Chen, and Q.-X. Chu, "Tunable cavity filter and diplexer using in-line dual-post resonators," *IEEE Trans. Microw. Theory Techn.*, vol. 70, no. 6, pp. 3188–3199, 2022.

[11] C. Arnold, J. Parlebas, and T. Zwick, "Reconfigurable waveguide filter with variable bandwidth and center frequency," *IEEE Trans. Microw. Theory Techn.*, vol. 62, no. 8, pp. 1663–1670, 2014.

[12] C. Arnold, J. Parlebas, R. Meiser, and T. Zwick, "Fully reconfigurable manifold multiplexer," *IEEE Trans. Microw. Theory Techn.*, vol. 65, no. 10, pp. 3885–3891, 2017.

[13] R. J. Cameron, C. M. Kudsia, and R. R. Mansour, *Microwave Filters for Communication Systems: Fundamentals, Design and Applications.* NJ: John Wiley & Sons, 2018.

[14] COMDEV, *COMDEV Space Group*. Canada: Cambridge, 2010.

[15] M. Daneshmand and R. R. Mansour, "RF MEMS satellite switch matrices," *IEEE Microw. Mag.*, vol. 12, no. 5, pp. 92–109, 2011.

[16] L. Pelliccia, P. Farinelli, V. Nocella, F. Cacciamani, F. Gentili, and R. Sorrentino, "Discrete-tunable high-Q E-plane filters," in *Proc. 43rd Eur. Microw. Conf. (EuMC)*, 2013, pp. 1215–1218.

[17] F. Gentili, F. Cacciamani, V. Nocella, R. Sorrentino, and L. Pelliccia, "RF MEMS Hairpin filter with three reconfigurable bandwidth states," in *Proc. 43rd Eur. Microw. Conf. (EuMC)*, 2013, pp. 802–805.

[18] L. Pelliccia, F. Cacciamani, P. Farinelli, and R. Sorrentino, "High-Q tunable waveguide filters using ohmic RF MEMS switches," *IEEE Trans. Microw. Theory Techn.*, vol. 63, no. 10, pp. 3381–3390, 2015.

[19] Y. Wang, J. Hu, and Y. Luo, "A terahertz tunable waveguide bandpass filter based on bimorph microactuators," *IEEE Microw. Wireless Compon. Lett.*, vol. 29, no. 2, pp. 110–112, 2019.

[20] B. Lee, S. Nam, and J. Lee, "Bandwidth tuning of resonator filter using reduced number of tunable coupling structures," *IEEE Trans. Microw. Theory Techn.*, vol. 67, no. 4, pp. 1496–1503, 2019.

[21] G. Basavarajappa and R. R. Mansour, "Design methodology of a high-Q tunable coaxial filter and diplexer," *IEEE Trans. Microw. Theory Techn.*, vol. 67, no. 12, pp. 5005–5015, 2019.

[22] J. Ossorio, J. C. Melgarejo, V. E. Boria, and M. Guglielmi, "On the integration of microwave filters and waveguide switches," *IEEE Microw. Wireless Compon. Lett.*, vol. 31, no. 3, pp. 265–268, 2021.

[23] G. Conciauro, M. Guglielmi, and R. Sorrentino, *Advanced Modal Analysis*. Chichester: John Wiley & Sons, 2000.

[24] J. W. Bandler, R. M. Biernacki, S. H. Chen, R. H. Hemmers, and K. Madsen, "Electromagnetic optimization exploiting aggressive space mapping," *IEEE Trans. Microw. Theory Techn.*, vol. 43, no. 12, pp. 2874–2882, Dec. 1995.

[25] J. E. Rayas-Sanchez, "Power in simplicity with ASM: Tracing the aggressive space mapping algorithm over two decades of development and engineering applications," *IEEE Microw. Mag.*, vol. 17, no. 4, pp. 64–76, Apr. 2016.

[26] J. Ossorio, J. C. Melgarejo, V. E. Boria, M. Guglielmi, and J. W. Bandler, "On the alignment of low-fidelity and high-fidelity simulation spaces for the design of microwave waveguide filters," *IEEE Trans. Microw. Theory Techn.*, vol. 66, no. 12, pp. 5183–5196, Dec. 2018.

[27] J. Melgarejo, M. Guglielmi, S. Cogollos, and V. E. Boria, "An efficient microwave filter design procedure based on space mapping," in *Proc. 50th Eur. Microw. Conf. (EuMC)*, Jan. 2020, pp. 212–213.
[28] M. Guglielmi and A. A. Melcon, "Novel design procedure for microwave filters," in *Proc. 23rd Eur. Microw. Conf. (EuMC)*, Sep. 1993, pp. 212–213.
[29] S. Cogollos, P. Micó, J. Vague, V. E. Boria, and M. Guglielmi, "New design methodology for multiband waveguide filters based on multiplexing techniques," in *IEEE MTT-S Int. Microw. Symp. Dig.*, June 2017, pp. 741–744.
[30] J. C. Melgarejo, S. Cogollos, M. Guglielmi, and V. E. Boria, "A new family of multiband waveguide filters based on a folded topology," *IEEE Trans. Microw. Theory Techn.*, vol. 68, no. 7, pp. 2590–2600, 2020.
[31] A. L. Allison, *The ITU and Managing Satellite Orbital and Spectrum Resources in the 21st Century*. Cham: Springer, 2014.
[32] R. J. Cameron and M. Yu, "Design of manifold-coupled multiplexers," *IEEE Microw. Mag.*, vol. 8, no. 5, pp. 46–59, Oct 2007.
[33] E. Sorolla, S. Anza, B. Gimeno, A. M. Pérez, C. Vicente, J. Gil, F. J. Pérez-Soler, F. D. Quesada, A. Álvarez Melcón, and V. E. Boria, "An analytical model to evaluate the radiated power spectrum of a multipactor discharge in a parallel-plate region," *IEEE Trans. Electron Devices*, vol. 55, no. 8, pp. 2252–2258, 2008.
[34] T. Pinheiro-Ortega, J. Monge, S. Marini, J. Sanz, E. Sorolla, M. Mattes, C. Vicente, J. Gil, V. E. Boria, and B. Gimeno, "Microwave corona breakdown prediction in arbitrarily-shaped waveguide based filters," *IEEE Microw. Wireless Compon. Lett.*, vol. 20, no. 4, pp. 214–216, 2010.

JUAN CARLOS MELGAREJO was born in Alicante, Spain in 1993. He completed his undergraduate degree, double masters and Ph. D. in Telecommunications Engineering at the Universitat Politècnica de València, Spain, in 2015, 2019 and 2021, respectively. He is currently working as a Machine Learning Engineer at Cambrian Intelligence. His main research interests are investigating microwave passive devices and new manufacturing techniques for satellite components.

JAVIER OSSORIO was born in Valencia, Spain, on March 24, 1992. He received the degree, double master and Ph. D. in telecommunications engineering from the Universitat Politècnica de València, Spain, in 2014, 2016 and 2021, respectively. He is currently working at Val-Space Consortium (VSC) laboratories at Universitat Politècnica de València specialized in Multipactor and Corona testing. His current research activities include EM simulations, efficient design and optimizations of waveguide filters and development of new tunable structure filters for satellite applications.

SANTIAGO COGOLLOS (M'07) was born in Valencia, Spain, on January 15, 1972. He received his "Ingeniero de Telecomunicación" degree and the Ph. D. degree from the Universitat Politècnica de València (UPV), Valencia, Spain, in 1996 and 2002, respectively. In 2000 he joined the Communications Department of the Universitat Politècnica de València, where he was an Assistant Lecturer from 2000 to 2001, a Lecturer from 2001 to 2002, and became an Associate Professor in 2002. He has collaborated with the European Space Research and Technology Centre of the European Space Agency in the development of modal analysis tools for payload systems in satellites. In 2005 he held a post doctoral research position working in the area of new synthesis techniques in filter design at University of Waterloo, Waterloo, Ont., Canada. His current research interests include applied electromagnetics, mathematical methods for electromagnetic theory, analytical and numerical methods for the analysis of microwave structures, and design of waveguide components for space applications.

MARCO GUGLIELMI was born in Rome, Italy, on December 17, 1954. He received the degree "Laurea in Ingegneria Elettronica" in 1979 from the University of Rome "La Sapienza", Rome, Italy, where in 1980 he also attended the "Scuola di Specializzazione in Elettromagnetismo Applicato". In 1981 he was awarded a Fulbright Scholarship in Rome, Italy, and an HISP (Halsey International Scholarship Programme) from the University of Bridgeport, Bridgeport, Connecticut, USA, where in 1982 he obtained an MS Degree in Electrical Engineering. In 1986 he received a PhD degree in Electrophysics from the Polytechnic University, Brooklyn, New York, USA. From 1984 to 1986 he was Academic Associate at Polytechnic University, and from 1986 to 1988 he was Assistant Professor in the same institution. From 1988 to 1989 he was Assistant Professor at the New Jersey Institute of Technology, Newark, New Jersey, USA. In 1989 he joined the European Space Agency as a Senior Microwave Engineer in the RF System Division of the European Space Research and Technology Centre (ESTEC), Noordwijk, The Netherlands, where he was in charge of the development of microwave filters and electromagnetic simulation tools. In 2001 he was appointed Head of the Technology Strategy Section of ESTEC where he contributed to the development of management processes and tools for the formulation of a European strategy for Space Technology Research and Development. In 2014 Dr. Guglielmi retired from the European Space Agency and is currently holding the position of Invited Senior Researcher at the Polytechnic University of Valencia, Valencia, Spain. Dr. Guglielmi has been elevated to the grade of Fellow of the IEEE in January 2013 "For contributions to multimode equivalent networks and microwave filter design".

ÁNGEL ANTONIO SAN-BLAS was born in Fortaleny, Valencia, Spain, in 1976. He received the Ingeniero de Telecomunicación and the Doctor Ingeniero de Telecomunicación degrees from the Universitat Politècnica de València, Valencia, Spain, in 2000 and 2008, respectively. From 2001 to 2002, he was a Researcher Assistant with the Departamento de Comunicaciones, Universitat Politècnica de València, where he was involved in the development of simulation tools for the analysis and design of waveguide devices. From November 2001 to March 2002, he was a Researcher with the Department of Electronics, Università degli Studi di Pavia, Pavia, Italy, where he was involved in the research project Millimeter-Wave and Microwave Components Design Framework for Ground and Space Multimedia Network (V European Framework Project). Since 2003, he has been an Associate Professor with the Departamento de Ingeniería de Comunicaciones, Universidad Miguel Hernández de Elche, Elche, Spain. His current research interests include the analysis and design of passive waveguide components for satellite communication systems. Dr. San-Blas also serves as an Editorial Board Member for the International Journal of Electronics and Communications (Elsevier).

JOAQUÍN F. VALENCIA-SULLCA was born in Lima, Peru, in March 1990. He received the Ingeniero de Telecomunicaciones degree from the Universidad Nacional de Ingeniería, Lima, in 2013, and the Master's degree in Communication Technologies, Systems and Networks, and a Ph. D. degree in Telecommunications Engineering from the Universitat Politècnica de València, Valencia, Spain, in 2016 and 2021, respectively. In 2022, he joined the Microwave Application Group (GAM), Institute of Telecommunications and Multimedia Applications (iTEAM) from the Universitat Politècnica de València. His current research interests include the analysis and design of passive components, electromagnetic simulations, and the efficient design and optimization of waveguide filters and their applications.

ANA VIDAL (M'01) was born in Valencia (Spain) in 1970. She received the Telecommunications Engineer and PhD degrees from the Universidad Politécnica de Valencia (Spain) and she stayed one year at University of Strathclyde, Glasgow (U.K.), under the Erasmus international exchange program. In 1993, she was involved in broadband communications development in the main research center of Telecom Portugal. She then became a Research Assistant with the Universidad Politécnica de Valencia. In 1995 and 1996, she held a Spanish Trainee position with the European Space research and Technology Centre (ESTEC)–European Space Agency (ESA), Noordwijk, The Netherlands, where she was involved in the study and implementation of software for synthetic aperture radar (SAR) image processing. In 1996, she returned to the Universidad Politécnica de Valencia, where she held several lecturing positions, and became an Associate Professor in 2001. Her current interests are Remote Sensing data classification, GNSS algorithms and numerical methods for the analysis and design of passive microwave components.

TILLMANN TRONSER was born in Pforzhei, Germany on April 14, 1990. He received the Bachelor of Science in Engineering and International Management at the Pforzheim University of Applied Science in 2015. He immediately joined the over 60 year old family business which specializes in the highest quality variable capacitors as well as customized RF components. After implementing a new ERP-System in the company he took over the sales department for the variable capacitors and custom RF components and became Executive Vice President. He successfully revitalized this branch and gained substantial market share. In 2020 he split off the variable capacitor and custom RF component bracket of the company to fully focus all of the power to these markets. He is now CEO of Tronser GmbH as well as board member and Vice President of Alfred Tronser GmbH.

VICENTE E. BORIA (S'91-A'99-SM'02-F'18) was born in Valencia, Spain, on May 18, 1970. He received his "Ingeniero de Telecomunicación" degree (with first-class honors) and the "Doctor Ingeniero de Telecomunicación" degree from the Universidad Politécnica de Valencia, Valencia, Spain, in 1993 and 1997, respectively. In 1993 he joined the "Departamento de Comunicaciones", Universidad Politécnica de Valencia, where he has been Full Professor since 2003. In 1995 and 1996, he was holding a Spanish Trainee position with the European Space Research and Technology Centre, European Space Agency (ESTEC-ESA), Noordwijk, The Netherlands, where he was involved in the area of EM analysis and design of passive waveguide devices. He has authored or coauthored 15 chapters in technical textbooks, 200 papers in refereed international technical journals, and over 250 papers in international conference proceedings. His current research interests are focused on the analysis and automated design of passive components, left-handed and periodic structures, as well as on the simulation and measurement of power effects in passive waveguide systems. Dr. Boria has been a member of the IEEE Microwave Theory and Techniques Society (IEEE MTT-S) and the IEEE Antennas and Propagation Society (IEEE AP-S) since 1992. He is also member of the European Microwave Association (EuMA), and has been the Chair of the 48th European Microwave Conference held in Madrid, Spain. He acts as a regular reviewer of the most relevant IEEE and IET technical journals on his areas of interest. He has been Associate Editor of IEEE Microwave and Wireless Components Letters (2013-2018) and IET Electronics Letters (2015-2018). Presently, he serves as Subject Editor (Microwaves) of IET Electronics Letters, and as Editorial Board member of International Journal of RF and Microwave Computer-Aided Engineering. He is also member of the Technical Committees of the IEEE-MTT International Microwave Symposium and of the European Microwave Conference.